Detection of Important Atmospheric and Surface Features by Employing Principal Component Image Transformation of GOES Imagery

DONALD W. HILLGER

NOAA/NESDIS/ORA/RAMMT, Fort Collins, Colorado

GARY P. ELLROD

NOAA/NESDIS/ORA/FPDT, Camp Springs, Maryland

(Manuscript received 15 November 2001, in final form 22 October 2002)

ABSTRACT

The detection of dust, fire hot spots, and smoke from the Geostationary Operational Environmental Satellite (GOES) is made easier by employing the principal component image (PCI) technique. PCIs are created by an eigenvector transformation of spectral band images from the five-band GOES Imager. The transformation is a powerful tool that provides a new set of images that are linear combinations of the original spectral band images. This facilitates viewing the explained variance or signal in the available imagery, allowing both gross and more subtle features in the imagery to be seen. Whereas this multispectral technique is normally applied to high-spatial-resolution land remote sensing imagery, the application is herein made to lower-spatial-resolution weather satellite imagery for the purpose of feature detection and enhancement. Features used as examples include atmospheric dust as well as forest and range fire hot spots and their resulting smoke plumes. The applications of PCIs to GOES utilized the three infrared window images (bands 2, 4, and 5) in dust situations as well as the visible image (band 1) in smoke situations. Two conclusions of this study are 1) atmospheric and surface features are more easily identified in multiband PCIs than in the enhanced single-band images or even in some two-band difference images and 2) the elimination of certain bands can be made either directly by inspection of the PCIs, discarding bands that do not to contribute to the PCIs showing the desired features, or by including all available bands and letting the transformation process indicate the bands that are useful for detecting the desired features. This technique will be increasingly useful with the introduction of new and increased numbers of spectral bands with current and future satellite instrumentation.

1. Introduction

The detection of certain important weather events and other environmental phenomena in satellite imagery is often quite challenging. Many such events are short lived and the usual spectral bands available on weather satellites when viewed alone are not optimal for looking at these meteorological phenomena. Instead, many of these events are detected only in image products created by weighted combinations of two or more spectral bands to obtain the features of concern. This raises the question of how best to detect these features. Usually, the satellite image analyst experiments to determine which spectral bands or band combinations are best for detecting what they are interested in seeing. Knowledge of the characteristics of various spectral bands helps in the process, but with the increasing numbers of spectral bands on new satellite instruments, the choices are sometimes beyond experimental reason and may be more a matter of serendipity.

In this paper, the technique of principal component image (PCI) transformation is shown to be a powerful tool for the analysis of multispectral weather satellite imagery. While the eigenvalue technique is normally applied to high-spatial-resolution (pixel dimensions smaller than 1 km) land remote sensing imagery (Taylor 1973; Madura et al. 1978), the current focus is on how the PCI transform is able to help with the analysis of various atmospheric and surface features from lower-spatial-resolution (1 km or greater) weather satellite imagery. The technique can be used to detect or discriminate many types of image features in multiband imagery: snow/cloud, volcanic ash (Hillger and Clark 2002a,b), cloud layers, land/water boundaries, cloud phase, and water vapor features in the atmosphere. Events examined in this paper are atmospheric dust as well as forest and range fire hot spots and their resulting smoke plumes.

The examples in this work focus on applications to the five-band Geostationary Operational Environmental

Corresponding author address: Dr. Don Hillger, NOAA/NESDIS/ORA/RAMMT, CIRA/Colorado State University, Fort Collins, CO 80523-1375.
E-mail: hillger@cira.colostate.edu

Satellite (GOES)[1] imager but have implications for other multispectral weather satellite imagery as well. Another useful application of PCI analysis is to assess multispectral image products from future satellites and instruments whose spectral bands are modified or expanded. For example, *GOES-12,* launched in 2001, has a new imager infrared band at 13.3 μm, replacing the 12.0-μm band (Hillger and Clark 2002b). In addition, the use of principal component analysis will be more important as the number of spectral bands increases, as is rapidly occurring in atmospheric remote sensing.

The following sections of this paper cover details about and applications of PCIs to the GOES imager, special cases constituting the main examples of atmospheric and surface phenomena studied, and conclusions from this analysis of GOES imagery using PCIs.

2. Basics of principal component image transformation

Principal components (PCs) have the ability to simplify multivariate data by reducing the dimensionality of the dataset (Gauch 1993). Features that are hidden in the data are brought out by PC analysis (Loughlin 1991). The PC theory dictates that the information content of the PCs is compressed into the PCs in order of descending significance, with the lower-numbered PCs containing the primary information content, and the higher-numbered PCs containing other information and noise. Both Morrison (1976) and Preisendorfer (1988) give good graphical representations of the PC transformation process. The process can be summarized as a translation and rotation of the original coordinate system into a new coordinate system that better reflects the principal modes of variability in the dataset being analyzed.

Because of its ability to simplify multispectral datasets, PC (or eigenvector/eigenvalue) analysis has been used extensively for the analysis of high-spatial resolution environmental (land and ocean) remote sensing imagery. However, the technique can also be used to analyze the information content of lower-spatial resolution weather satellite imagery (Hillger 1996a,b). Regardless of the intended application, the technique determines which part of the multispectral signal is common to all the images (spectral bands) and separates that information from other image information that is sensed only by image differences or multiple image combinations. Whereas the original images may (and often do) contain redundant information, the PCIs contain the independent signal separated out of the original images. This allows the image analyst to see the independent components of multispectral imagery.

[1] The current series of GOES carries two multispectral remote sensing instruments, a 5-band imager and a 19-band sounder.

a. PCI application to satellite imagery

The process of transforming multiband satellite imagery into PCIs is based on statistics generated from the images. Consider a set of imagery from N bands, viewing a scene at M horizontal locations (pixels, which include data collected in scan lines and with a large number of samples in each line). At each pixel or location a vector of length N, denoted by $\mathbf{B}$, can represent the multiband imagery. A special linear transformation can be applied to provide a new vector of length N, denoted PCI as follows:

$$\text{PCI} = \mathbf{E} \times \mathbf{B}, \tag{1}$$

where $\mathbf{E}$ is an $N \times N$ matrix. For PCIs, the rows of $\mathbf{E}$ are the eigenvectors of the symmetric $N \times N$ covariance matrix with elements composed of covariances among the bands (summed over M pixel locations). The covariance matrix is generated from the imagery (or a subset of the imagery) being analyzed, and the eigenvectors are determined using a standard mathematical package for diagonalizing that matrix. The covariance matrix explains the relationships among the band images, allowing the eigenvector transform to parse that information into the PCIs. This parsing separates common and difference information from the multispectral imagery. The common information is concentrated into the PCIs in order of decreasing explained variance (the square of the eigenvalue), with PCI-1 containing most of the variance, and lesser variance in higher-numbered PCIs. The result of the eigenvector transformation is a restructuring of the satellite information into as many PCIs as there are available spectral band images. (The PCIs can have no more degrees of freedom than the band images that are input.) The sum of the explained variances of the PCIs is equal to the sum of the explained variances of the original images, the same information content as the original imagery expressed in a new form.

The PCI concept is easier to explain when simplified to a small number of images or dimensions. In the simplest two-dimensional case, two band images (b1 and b2) are transformed into two PCIs (pci1 and pci2), using

$$\text{pci1} = \mathbf{e}1 \cdot \text{b1} + \mathbf{e}2 \cdot \text{b2}, \quad \text{and} \tag{2}$$

$$\text{pci2} = \mathbf{f}1 \cdot \text{b1} + \mathbf{f}2 \cdot \text{b2}, \tag{3}$$

where $\mathbf{e}$ and $\mathbf{f}$ are linear transformation vectors (eigenvectors, or rows in the eigenvector matrix $\mathbf{E}$) used to transform each pixel (or picture element) in the original band images into two PCIs. The individual es and fs (eigenvector coefficients) can be positive or negative, for adding or subtracting the bands, as required by the transformation from bands into PCIs. With only two input bands, pci1 contains the information that is common to the b1 and b2 images (an image sum), and pci2 contains the information that is not shared, or that differs between, the b1 and b2 images (an image difference). The three-band case can be visualized as a transformation of axes in three-dimensional space. For increas-

TABLE 1. Basic information on the GOES imager.

GOES imager band	Wavelength range (μm)	Spatial resolution (km) at nadir (east–west × north–south)	Meteorological objective
1	0.55–0.75	0.6 × 1	Cloud cover and surface features during the day
2	3.8–4.0	2.3 × 4	Cloud phase (day and night)
3	6.5–7.0	2.3 × 8	Upper-level water vapor
4	10.2–11.2	2.3 × 4	Surface or cloud-top temperature
5	11.5–12.5	2.3 × 4	Surface or cloud-top temperature and low-level water vapor

ing numbers of images the transformation is increasingly harder to visualize.

b. The GOES imager and PCIs

The PCI examples in this paper focus on the GOES imager. Five GOES satellites (*GOES-8, -9, -10, -11,* and *-12*) in the current GOES-I series have been launched since 1994. Two of the satellites are operational at any time, with imagery from one satellite covering the eastern United States (subpoint 75°W), and imagery from the other covering the western United States (135°W). The GOES imager and sounder instruments have been used to detect a wide range of meteorological phenomena and surface properties via their multispectral capabilities (Holt and Olson 1999). Many of those features are detected by manipulation of the individual band images to generate product images (e.g., cross-spectral differences in reflected solar radiation and radiation emitted by the earth). One such image combination most useful at night is the GOES fog product generated by subtracting band-2 temperatures from band-4 temperatures (Ellrod 1994). During the day, significant differences between images in the two bands are due to the presence or absence of the reflective component of radiation in shortwave band 2 (Dills et al. 1996). While many products are simple subtractions of two images, it is often the case that combinations of more than two bands are needed to expose the more complex information content in GOES imagery.

Knowledge of cloud/atmosphere/surface optical properties is helpful in determining the kinds of image products that are possible from multispectral satellite data. Table 1 contains some basic information on the five-band GOES imager. The wavelength range is listed in the second column, the spatial resolution is indicated in the third column, and the last column lists the meteorological phenomena that the GOES images were designed to sense. The GOES pixels are square, but they are oversampled along the scan line (basically east–west orientation), having approximately twice the spatial sampling in this direction compared to the north–south direction (Menzel and Purdom 1994), resulting in the spatial resolutions given in the table. Some of the applications in this paper use such oversampled imagery, which appears stretched in the east–west direction when displayed. In other cases, when every other element in each line is used (sampled) the imagery can be displayed at approximately equal east–west and north–south resolutions. In either case, the north–south resolution is normally used when referring to the spatial resolution of GOES.

For the purposes of PCI analysis, where the images are effectively added and subtracted, the spatial resolution of all the images needs to be equalized. The options range from sampling (or averaging) the image pixels to that of the lowest resolution band (8 km for the water vapor image), or to replicating the image pixels to that of the highest resolution band (1 km for the visible image). Because three of the GOES spectral band images are available at 4-km resolution, often the best use of the imagery involves generating PCIs at this resolution. In this case the 1-km visible image is converted into 4-km resolution by sampling every fourth scan line and element. (Note that pixel sampling is used because it is simpler and faster and inherent in the image processing used, but pixel averaging is probably a better way to combine images at different spatial resolutions. The results, however, are not expected to be significantly different between the two methods because most atmospheric features are larger than the spatial resolution of GOES.) Also, the line resolution of the water vapor image, being half that of the other infrared images, is replicated to 4-km resolution by duplicating every scan line to generate 4-km imagery; the infrared element resolutions being equal.

GOES data are available in several different measurement units. The basic units supplied to users are 10-bit GOES variable data format (GVAR) counts (0–1023), a digital scale that has a fixed and linear relationship to radiance units measured directly by GOES instrumentation. Other possible measurement units include: calibrated radiances, temperatures (for the infrared images) or albedos (for the visible image), and 8-bit display counts (Weinreb et al. 1997). Unlike radiances, temperatures are nonlinearly related to GVAR counts. In spite of this difference, PCIs created from GVAR counts (or radiances) and those created from infrared temperatures are not significantly different. The 8-bit form of satellite imagery is common because many contemporary display systems are 8 bits deep. Because 8-bit data lack the precision of the original 10-bit GVAR data, PCIs generated from the highest bit depth data (GVAR counts) are preferred (Hillger 1999).

Many interesting examples of PCIs created from the five-band GOES imager are possible. The technique is useful for detecting and enhancing many types of atmospheric and surface phenomena (Hillger and Ellrod 2000). While the interpretation of the PCIs is fairly stable and predictable when they are created using all available bands on a large spatial scale, significant differences in interpretation occur between day and night when the presence or absence of reflected solar radiation is an important factor in GOES bands 1 and 2 (Hillger 1996a,b; Hillger and Clark 2002a,b). For this reason PCIs are not necessarily the best technique for direct operational applications, but can prove useful for determining combinations of the available band images for the detection of various atmospheric and surface features.

3. Special cases for PCI analysis of GOES

The following sections present intensive analysis of PCIs in special cases of dust, and fire hot spots and their associated smoke plumes. The intent is to provide the reader with an understanding of a few types of meteorological features and situations for which PCI analysis works better than more traditional approaches (e.g., simple image enhancement or image differences).

a. PCI analysis of atmospheric dust

One of the important atmospheric features observable in satellite imagery is blowing dust (Fraser 1976). The detection of dust storms is important because of the resulting reduced visibility and associated winds. Atmospheric dust storms can occur over the Great Plains during high-wind events (Lee and Tchakerian 1995). Frequently these events are associated with cold fronts, causing the most widespread dust storms (Pollard 1978).

1) FIRST DUST CASE

Figure 1 contains imagery from all five *GOES-10* bands for a dust storm that occurred on 27 March 1998 over a large portion of northern Texas. This set of images, collected at 2145 UTC and displayed at 4-km resolution, contains only slight indications of dust in the band-1 and band-4 images in the clear air south of the cloudy region over Oklahoma associated with a low pressure center. Surface weather reports plotted over the visible image (band 1, upper left-hand panel) indicate blowing dust (BD) and haze (H) at some observation locations both within and outside the discernable plume. These reports persisted for several hours around the image time. The actual extent of dust spans from central Oklahoma, arcs to the south and west, and extends to New Mexico. During the dust storm sustained winds at the surface in northern Texas were westerly at 15 m s^{-1}, with wind gusts near 20 m s^{-1}.

Better indications of the dust storm than the original images in Fig. 1 are provided by the PCIs in Fig. 2. This figure contains five PCIs at 4-km resolution generated for this case from all five *GOES-10* images. The first component image (PCI-1, upper left-hand panel) indicates the overall cloud picture. The dust area appears most isolated from other image features as the white area in the center of PCI-5 (lower left-hand panel). The dust extent agrees with the surface reports in the first panel of Fig. 1, although not all locations affected by the dust have issued reports of dust. The dust area in PCI-5 is also seen in PCI-4 (middle right-hand panel), in a negative sense, as an area slightly darker than the image background.

Table 2 can be used to understand the makeup of the PCIs in Fig. 2. Each PCI is quantified by the explained variance of the contributing GOES bands (the square of the eigenvector coefficient associated with each band). The explained variance for each PCI summed over the five bands is 100%, indicative of the conservation of variance inherent in the PCI technique. Also, each PCI in general contains both positive and negative contributions from the bands (determined by the sign of eigenvector coefficient for that band). Positive numbers (not in parentheses) indicate bands that make positive contributions toward a particular PCI. Conversely, negative numbers (in parentheses) indicate bands that make negative contributions toward that PCI. For example, PCI-1 is a combination of positive contributions from GOES bands 2–5, and a negative contribution from band 1 (visible). There is typically a negative correlation between the information in the visible and infrared bands. Clouds are the brightest objects (high GVAR counts) in visible imagery and at the same time the coldest objects (low GVAR counts) in infrared imagery. This inverse relationship, which shows up in the way the bands are added and subtracted to generate the PCIs, is masked when the images are displayed so that clouds appear white in both visible and infrared imagery.

PCI-5, which shows the dust clearly as white, is composed almost exclusively of a difference between GOES band-4 and band-5 images. PCI-4, which shows the dust very slightly, has its most significant (positive) contribution from the band-2 image, and negative contributions from the other bands. A theoretical study by Takashima and Masuda (1987) has shown that dust has a larger emissivity in a dirty spectral window (i.e., GOES band 5) than in the normal window (i.e., GOES band 4), causing a difference in the radiative temperatures between the two bands. The temperature difference can be either positive or negative, depending on the type of dust and the atmospheric level of the dust. The study did not include the shorter wavelength infrared region of GOES band 2, but it appears from a comparison of PCI-4 (which includes band 2) with PCI-5 (the band 4 − 5 difference) that the band-2 image, in combination with the GOES longwave images, is not as suitable for detecting this dust storm as the difference between the longwave infrared images.

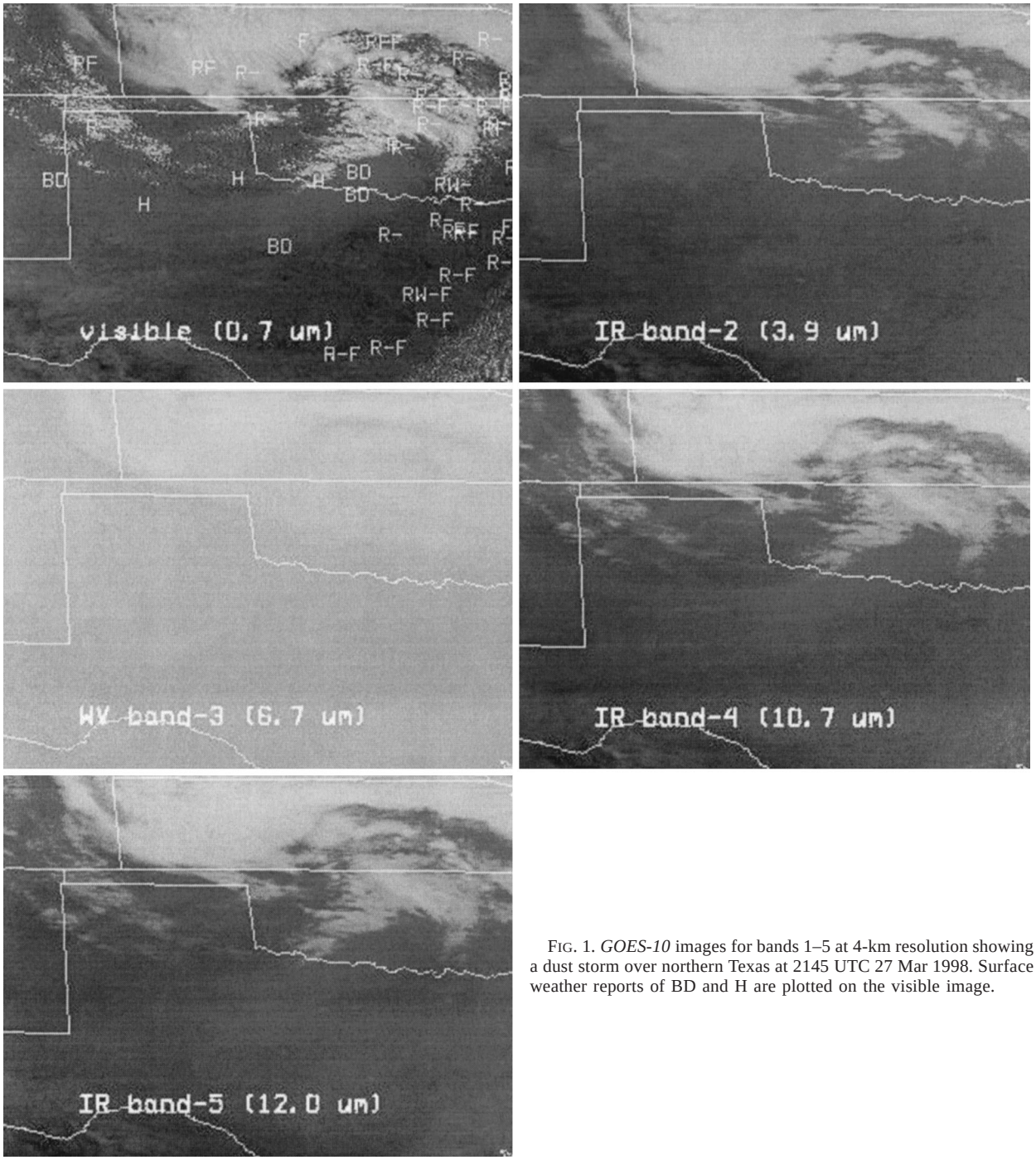

FIG. 1. *GOES-10* images for bands 1–5 at 4-km resolution showing a dust storm over northern Texas at 2145 UTC 27 Mar 1998. Surface weather reports of BD and H are plotted on the visible image.

The remaining PCIs, PCI-2 and -3, are composed of large contributions from the shortwave infrared (band 2) and the water vapor (band 3), respectively, but with smaller contributions from some of the other bands. PCI-2 and -3 appear to emphasize cloud edges, probably due to subpixel variations in temperature, features that are common in PCIs when generated over highly variable cloud fields. In addition, PCI-3 shows water vapor and temperature variations across the image that may be seen in contrast-stretched band images.

At this point, an attempt is made to isolate the dust storm signal to a subset of the GOES images. This is to prove that the bands of little or no value can be eliminated from the analysis without consequence. First, the band-1 image was eliminated because PCI-2, which contains the largest contribution from band-1 image,

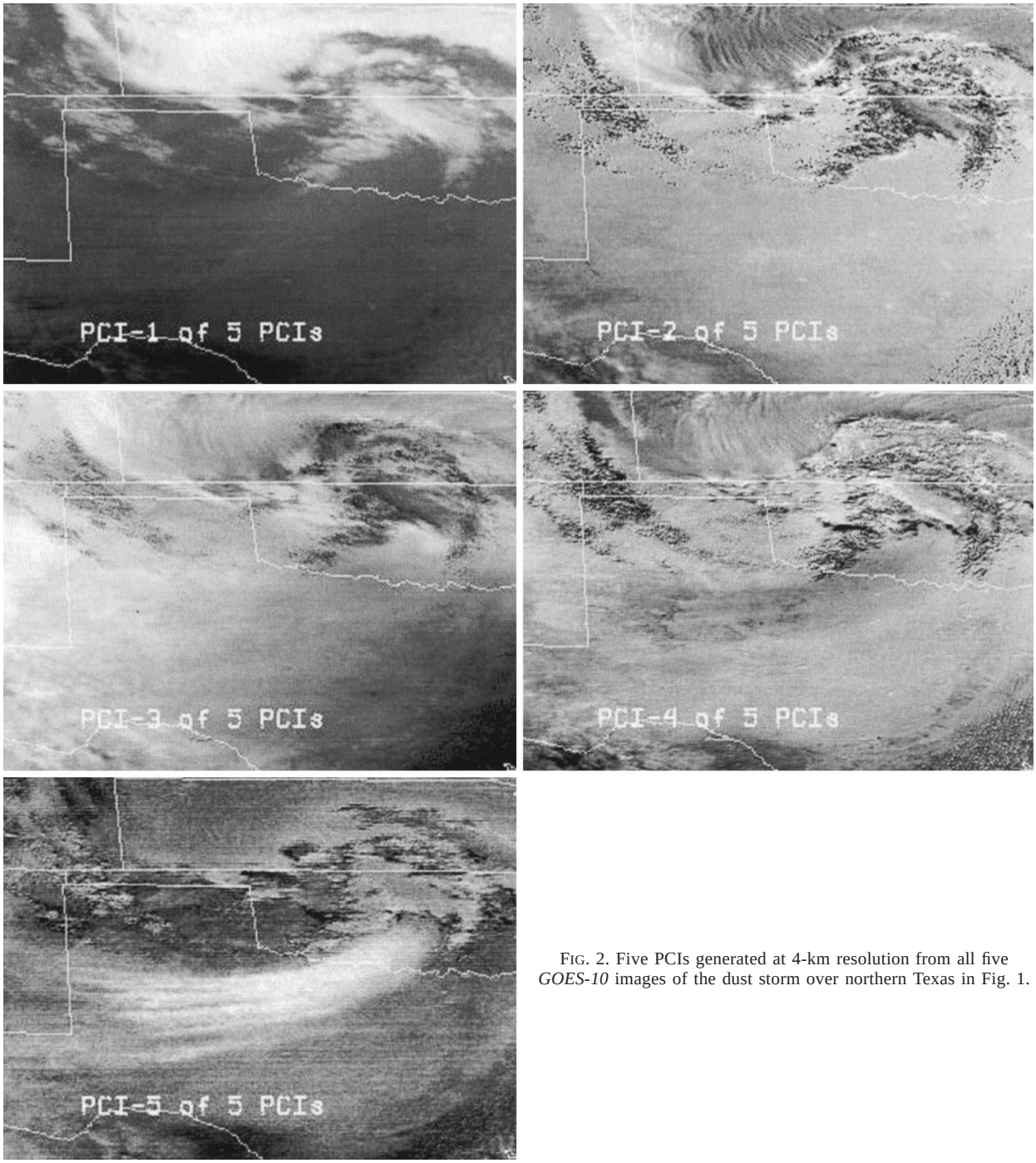

FIG. 2. Five PCIs generated at 4-km resolution from all five *GOES-10* images of the dust storm over northern Texas in Fig. 1.

does not indicate the presence of the dust. Also, the band-3 image was eliminated because PCI-3, which contains the largest contribution from the band-3 image, does not indicate the presence of the dust area. Figure 3 contains the three PCIs generated from the three remaining GOES images (bands 2, 4, and 5). In this new set of PCIs, the dust area appears white and most predominant in PCI-3 (lower left-hand panel) and again slightly dark in PCI-2 (upper right-hand panel). These two PCIs are nearly identical to PCI-4 and PCI-5 for the five-band analysis above.

Also shown in the lower right-hand panel of Fig. 3 is a simple split-window GOES band-difference image, a product that is normally be used to detect dust in GOES imagery. This image product is the band $5 - 4$ difference in temperature units, stretched to fill the available image counts. The bands are differenced in that order to make the dust appear white. The image is quite

TABLE 2. Explained variances and signal-to-noise ratios of PCIs generated from all five GOES bands for 2145 UTC 27 March 1998 dust case over northern Texas.

PCI No.	Explained variance (%) and sign (negatives in parentheses) of GOES and contributions					PCI explained variance (%)	PCI signal-to-noise ratio
	1	2	3	4	5		
1	(12.0)	12.5	4.5	33.8	37.3	93.6	65.4
2	80.6	14.5	(0.1)	2.3	2.4	4.1	11.8
3	3.1	(9.3)	87.4	(0.2)	(~0)	1.9	18.4
4	(4.3)	63.5	(7.9)	(10.0)	(14.1)	0.4	5.3
5	~0	(0.1)	~0	53.7	(46.1)	0.1	3.9

similar to PCI-3 in the lower left-hand panel, which is not surprising based on what we shall see about the bands that contributed to PCI-3.

Table 3 is formatted similarly to Table 2, but for PCIs generated from GOES bands 2, 4, and 5 only. The band makeup of PCI-3 is almost identical to that of PCI-5 in Table 2, with by far the largest contributions from bands 4 and 5. Similarly, PCI-2 in Table 3 is composed mainly of band 2 (84.6%), as is PCI-4 in Table 2 (63.5%). All three remaining bands are important contributors to both PCI-2 and PCI-3, but the best indication of dust is PCI-3—the difference between the band-4 and band-5 images.

By comparing PCI-2 (upper right-hand panel) and PCI-3 (lower left-hand panel) in Fig. 3 with PCI-4 and PCI-5 in Fig. 2, it appears that both sets of PCIs are good for discerning the extent of the dust, and that the band-1 and band-3 images were not critical to the analysis. The only surprise was that the visible image did not contribute significantly to identifying the dust, especially because there appear to be slight indications of the dust cloud in this band. Typically dust particles are

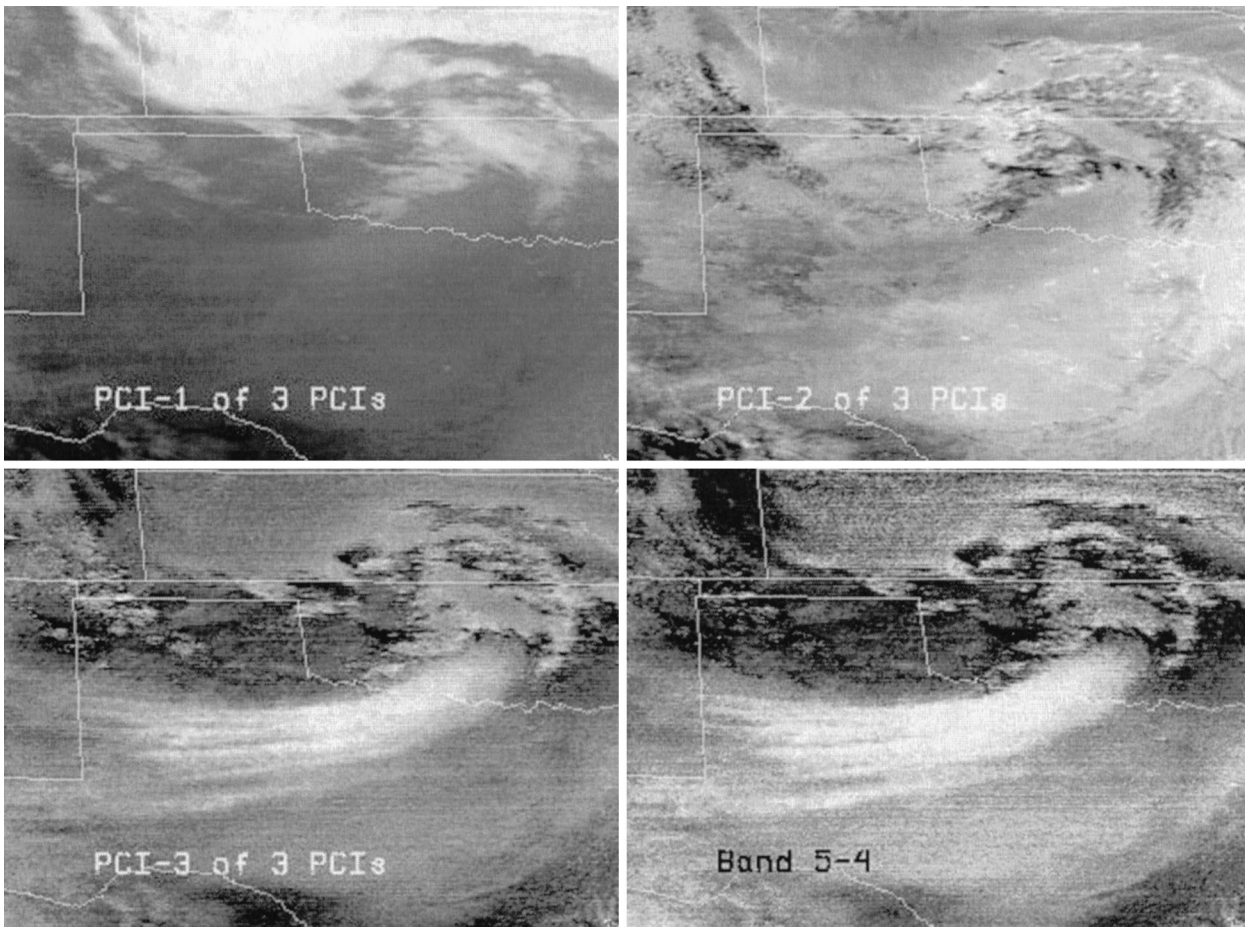

FIG. 3. Three PCIs generated at 4-km resolution from selected *GOES-10* images (bands 2, 4, and 5) of the dust storm over northern Texas in Fig. 1. (lower right) The simple GOES band 5 − 4 difference image is shown for comparison.

TABLE 3. Same as Table 2, but generated from GOES bands 2, 4, and 5 only.

PCI No.	Explained variance (%) and sign (negatives in parentheses) of GOES band contributions			PCI explained variance (%)	PCI signal-to-noise ratio
	2	4	5		
1	15.2	40.2	44.5	99.0	54.6
2	84.6	(6.0)	(9.4)	0.9	8.0
3	(0.1)	53.7	(46.1)	0.1	4.0

quite small and are harder to detect at shorter visible wavelengths than at longer infrared wavelengths, where they influence infrared heating and cooling of the atmosphere. This means that nighttime detection of dust should not be hindered by the lack of visible imagery. The poor contribution by the visible image, however, is not the case for all atmospheric phenomena, as will be seen in the smoke detection cases to be presented.

The last two columns of Tables 2 and 3 present additional quantitative analysis of the PCIs. The explained variances in the second-to-last column indicate that the higher-numbered PCIs that show the dust contain only a small fraction (less than 1%) of the total explained variance in the original GOES bands. The last column is an analysis of the signal-to-noise ratio (SNR) of each PCI. This was accomplished by structure function analysis to get both the signal and noise levels of the imagery (Hillger and Vonder Haar 1988). SNRs are quantitative measures of the contrast of image features (including dust) to the image background. An SNR greater than 1 indicates that an image contains a signal that is distinct from the noise background. In this case, a value of 3.9 or greater for the last PCIs is sufficient to allow the extent of the dust to be easily seen even though the explained variances are low for those same PCIs.

From this first case it is clear that the split-window band difference (between bands 4 and 5) in PCI-3 is the most useful for dust detection. This is confirmed by comparison to the simple band 5 − 4 difference image. The GOES split-window difference has likewise been found useful for detecting Saharan dust by Ellrod (1995) and others. Only a minimal dust signal was observed in PCI-2, with the majority of its signal from band 2. Because the dust in this case was easily observed in a simple two-band difference (as in PCI-3, but not in any of the other PCIs), the multiband differences in the other PCIs did not provide any advantage. Rather, the PCIs confirmed that the two-band difference is sufficient for detecting dust in this case.

2) SECOND DUST CASE

Figure 4 contains *GOES-8* images for bands 1, 2, 4, and 5 for 2155 UTC 19 April 1995 (band 3 is not used in the analysis and is not shown). In this case, the dust storm is associated with a frontal passage indicated by an arc of clouds extending south and west across central Texas. Surface weather reports plotted over the visible image (band 1, upper left-hand panel) indicate BD at some observation locations behind the front. The post-frontal dust storm covers a large portion of the Texas Panhandle to the west and north of the surface front. Only the band-1 and band-4 images (upper left-hand and lower right-hand panels, respectively) provide slight indications of the dust.

Rather than showing both five-band and three-band PCIs, only the three-band PCIs (using bands 2, 4, and 5) will be shown and discussed. The decision to eliminate the other GOES bands was based on PCIs generated with and without these images, because the PCIs with major contributions from the band-1 and band-3 images did not indicate the dust storm, as was true in the first case.

Figure 5 contains the PCIs for this second dust case. PCI-3 (lower left-hand panel) shows the dust area as white, similar to the first case (compare with PCI-3 in Fig. 3). What is different about this case is that PCI-2 (upper right-hand panel) shows the dust as a much darker area than PCI-2 in Fig. 3. Comparing Table 4 with Table 3, the PCIs are generated from very similar combinations of bands 2, 4, and 5. The PCIs of importance have low explained variance, yet good SNRs. This exemplifies the power of PCI analysis to bring forth subtle yet meaningful information from satellite imagery.

Also shown in the lower right-hand panel of Fig. 5 is a simple GOES split-window band 5 − 4 difference image for comparison to the PCIs. This image product, generated as in Fig. 3, is quite similar to PCI-3 in the lower left-hand panel, because PCI-3 is composed of significant contributions from only those two bands. However, in the simple band-difference image, the dust appears to be more widespread to the southwest. This is where the dust signal in PCI-2 helps resolve this discrepancy in the extent of the dust between PCI-3 and the two-band difference image, limiting the dust to the area indicated by the surface reports that were plotted in Fig. 4.

The larger signal of the dust in PCI-2 for this case is likely due to quantifiable differences between the situations. Because the observation dates and times are nearly identical, the only real difference is the geometric viewing angle. *GOES-8* imagery for this case is viewing Texas from the southeast, whereas *GOES-10* imagery for the previous case is viewing the same region from almost directly south (subpoint 105°W on that date during initial testing of the satellite). The scattering angle between the sun and the satellite at the late afternoon time of observation is much larger for *GOES-8* (74°) than for *GOES-10* (40°). Because most atmospheric particulates scatter preferentially in the forward direction, this larger angle is likely the cause for the greater signal for the dust in the second case. Other possible differences could be the height of the dust or the size distribution and concentration of dust particles between the two cases, neither of which is known. Aside from the

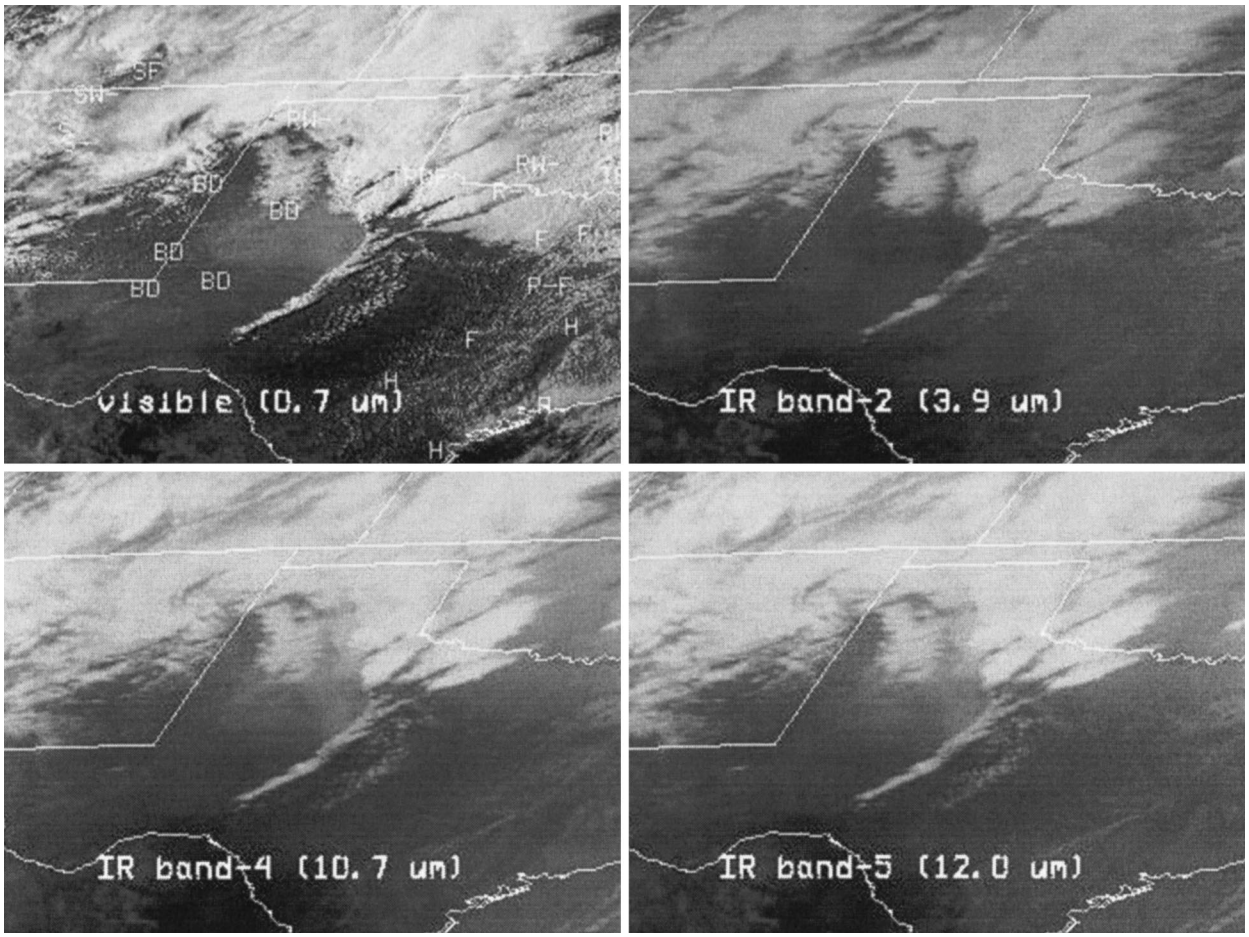

FIG. 4. *GOES-8* images for bands 1, 2, 4, and 5 at 4-km resolution showing a postfrontal dust storm over the Texas Panhandle at 2155 UTC 19 Apr 1995. Surface weather reports of BD are plotted on the visible image.

view angle difference, without in situ details on the dust, it cannot be determined what is the true cause of the difference between the cases.

Because PCI-2 yielded a better enhancement of the dust for this second case, this indicates that GOES band 2 is more important for dust detection than indicated by the first dust case. The simple split-window band difference alone detected the dust, but not without ambiguity. There is additional information on the dust in band 2 as indicated by its large contribution to PCI-2. In this case, PCIs indicated that image combinations other than the split-window difference are helpful for detecting the presence and extent of dust in the atmosphere.

b. PCI analysis of smoke plumes and fire hot spots

In the following cases the emphasis will switch to fires and their associated smoke plumes. These are different phenomena than the dust storms already examined, showing that different combinations of bands are important.

1) FIRST SMOKE AND FIRE CASE

The first case to be analyzed consists of two biomass/forest fires in the Los Padres National Forest in the mountains north of the Los Angeles basin in southern California on 31 August 1999. Figure 6 contains images from *GOES-10* bands 1, 2, 4, and 5 at 2046 UTC for this case. Because of the small area covered by the fires, all the images are presented at 1-km resolution (i.e., pixel replication of the 4-km infrared imagery). All images are contrast-stretched (by histogram equalization) to enhance features otherwise hard to discern in the original GOES bands. The water vapor image (band 3) is not shown and is not used in the subsequent analysis because the maximum absorption and emission in the water vapor band is from the middle levels of the atmosphere, whereas the smoke and fires are mainly low-level and surface phenomena.

Arrows point to both fire hot spots, which are most apparent as darker pixels in the shortwave infrared image (band 2, upper right-hand panel) of Fig. 6. The (left) western fire appears to be more completely surrounded

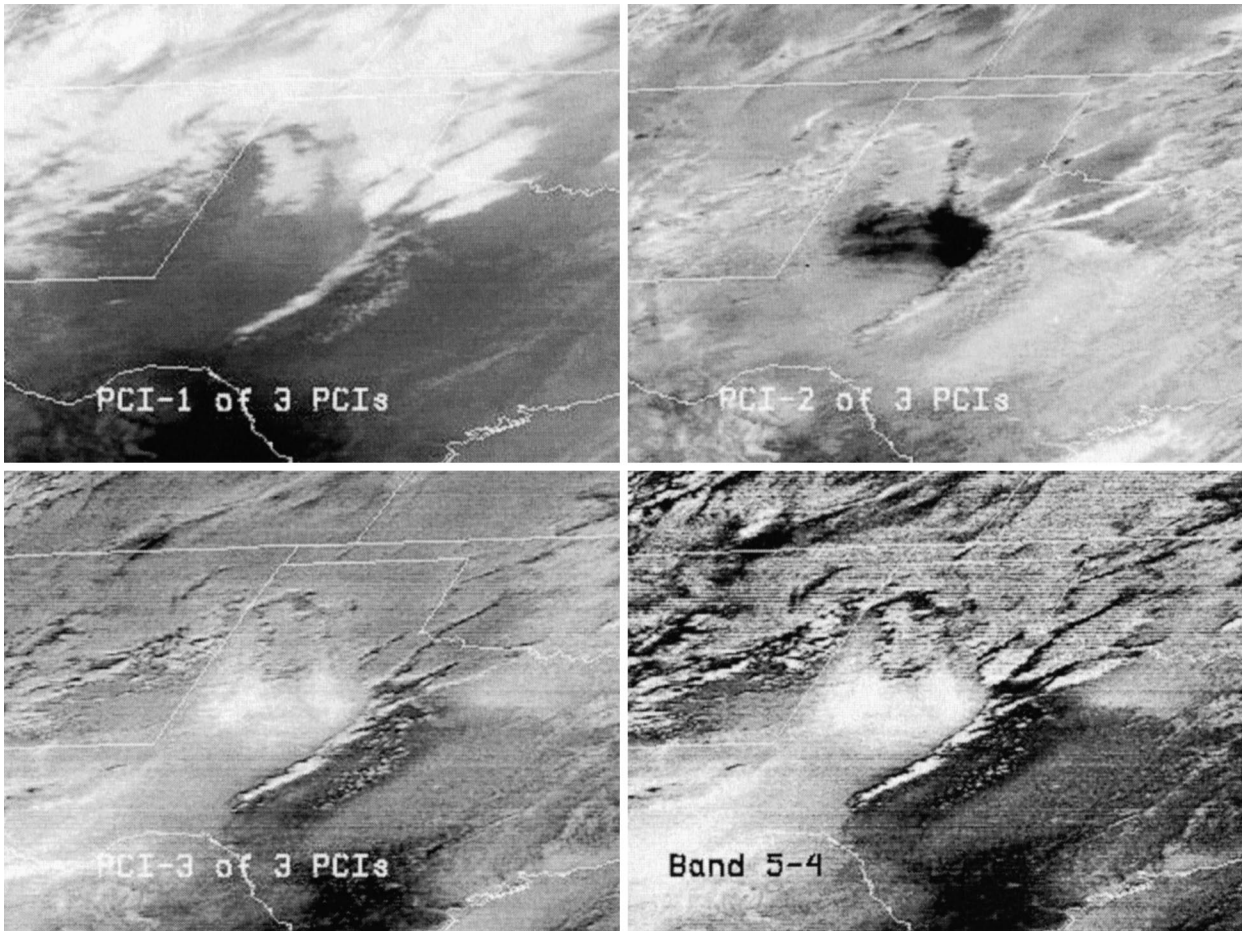

FIG. 5. Three PCIs generated at 4-km resolution from selected *GOES-8* images (bands 2, 4, and 5) of the postfrontal dust storm over the Texas Panhandle in Fig. 4. (lower right) The simple GOES band 5 − 4 difference image is shown for comparison.

by colder (whiter) pixels than the (right) eastern fire. The smoke plume from the eastern fire appears colder (whiter in the infrared imagery) than the surrounding pixels and extends from the fire toward the northeast in this image, following the prevailing wind direction at the time. However, without knowledge of the terrain, the colder smoke plume could easily be confused with the higher, colder terrain (noted on the band-4 image) extending east–west across the fire hot spots.

The longwave band images (bands 4 and 5; two lower panels) do not indicate the fire hot spots as readily as the band-2 image. This is due to the increased sensitivity of the shortwave band (band 2) to warm scenes compared to the longwave bands. The two fires have similar radiative temperatures (320 K averaged over the hottest pixel), but the eastern fire appears hotter (darker) in these two images due to the contrast of the fire pixels to the surrounding pixels. While the smoke plume from the eastern fire is more apparent, probably due to its greater density, there is a slight indication of smoke from the western fire extending toward the northeast. Lastly, the visible image (band 1, upper left-hand panel) has only slight indications of a smoke plume from the eastern fire, and the western fire is associated with a white area that may be a patch of dense smoke (both are indicated by arrows and question marks); otherwise, the scene is largely cloud free.

Figure 7 is the PCI analysis generated for this case at 1-km resolution from the four *GOES-10* images (bands 1, 2, 4, and 5) in Fig. 6. PCI-1 has indications of the fire hot spots and the smoke plumes, as well as other terrain features. These features look similar in the band-2, -4, and -5 images; therefore, PCI-1 collects the common signal from among the GOES bands.

TABLE 4. Explained variances and signal-to-noise ratios of PCIs generated from GOES bands 2, 4, and 5 only for 2155 UTC 19 April 1995 postfrontal dust storm over the Texas Panhandle.

PCI No.	Explained variance (%) and sign (negatives in parentheses) of GOES band contributions			PCI explained variance (%)	PCI signal-to-noise ratio
	2	4	5		
1	15.1	40.8	44.0	99.0	110.2
2	84.8	(7.8)	(7.3)	0.9	8.7
3	~0	51.3	(48.7)	0.1	4.2

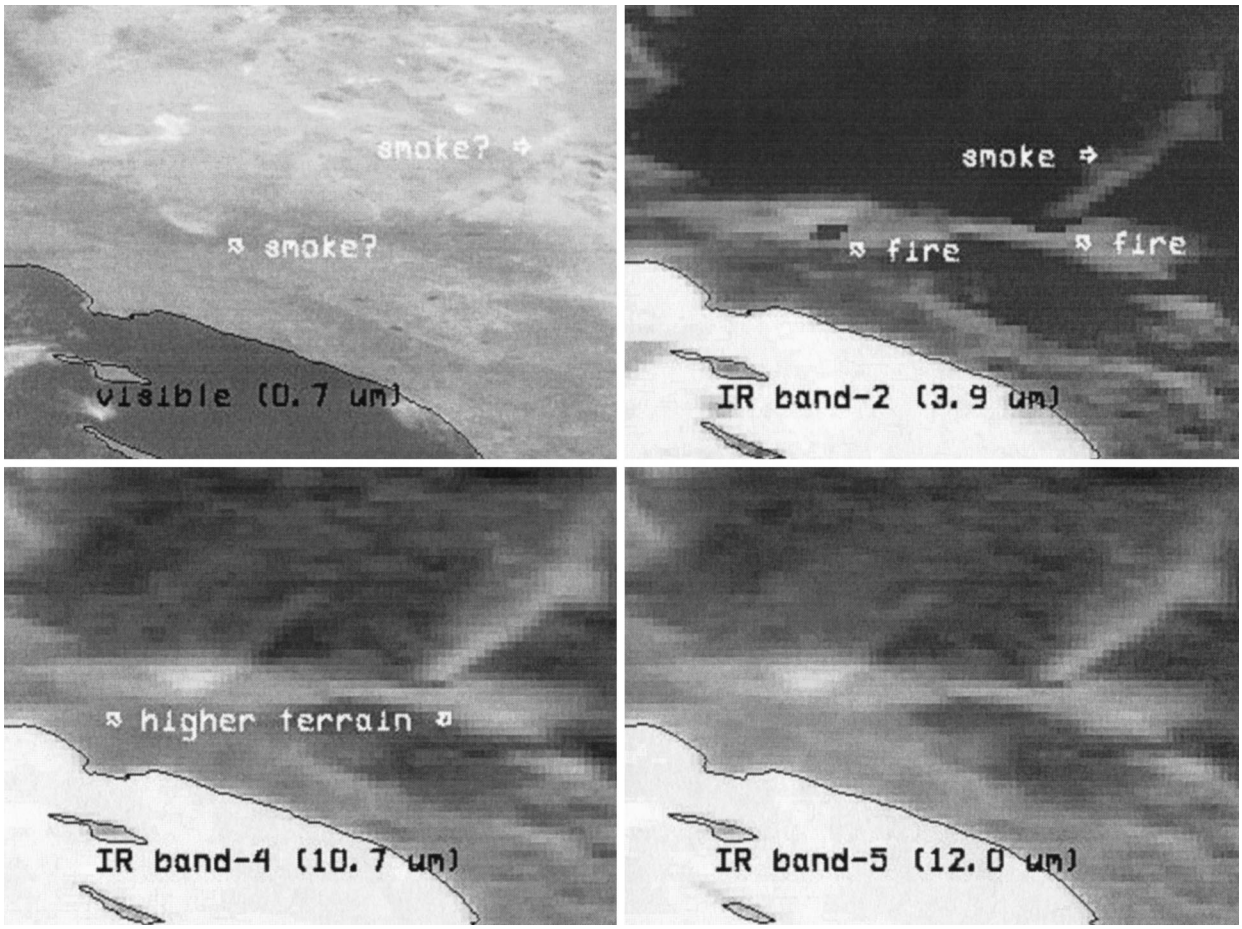

FIG. 6. *GOES-10* images for bands 1, 2, 4, and 5 at 1-km resolution showing two fires in the mountains north of the Los Angeles basin in southern California at 2046 UTC 31 Aug 1999. The two fire hot spots and smoke plume from the eastern fire are noted on the band-2 image. All images are contrast stretched to enhance features that are otherwise hard to discern.

The best indication of the fires in Fig. 7 is in PCI-3 (middle left-hand panel). This image combination clearly depicts the fire hot spots as black and suggests the presence of smoke plumes from not just the eastern fire but from the western fire as well, extending toward the northeast from each fire hot spot. As indicated in Table 5, PCI-3 heavily utilizes the shortwave infrared image (band 2) that is more sensitive to hot spots than the longwave infrared images (bands 4 and 5). The band-2 image has a long history of being used for fire detection, especially when an image difference is generated between the shortwave and longwave infrared bands (Matson and Dozier 1981). To confirm, the lower left-hand panel contains a simple GOES band 2 − 4 shortwave–longwave difference image for comparison to the PCIs. The image product contains fire and smoke features (white areas) that are somewhat similar to those in the PCIs, however, the multiple differences available in the PCIs show features that would only be observed in additional band differences.

PCIs 2 and 4 do not show the fire hot spots as well, but contain indications of smoke. PCI-2 (upper right-hand panel) in Fig. 7 is nearly an inverted version of the visible image (band 1) in Fig. 6. Table 5 verifies that there is little contribution from the other bands in this PCI. PCI-2 shows the smoke areas as dark, both the dense smoke patch from the western fire and the thinner smoke plume from the eastern fire, along with other cloud and surface features not seen as easily in the visible image alone. PCI-4 (middle right-hand panel) shows both fire hot spots and the smoke from the eastern fire as white. The signal in PCI-4, mainly from split-window differencing the two longwave infrared (band 4 and 5) images, appears similar to that for high-level (thin) cirrus cloud. Thin clouds show up in the image difference due to differential transmittance of upward radiation (due to different optical thickness) between the two spectral bands (Arking and Childs 1985).

All of the PCIs have some indication of either the fire hot spots or smoke plumes. These features, although detectable in some of the original band images, are better depicted in the PCIs than in the simple two-band shortwave–longwave difference shown. All four input GOES bands contributed significantly to the multiband

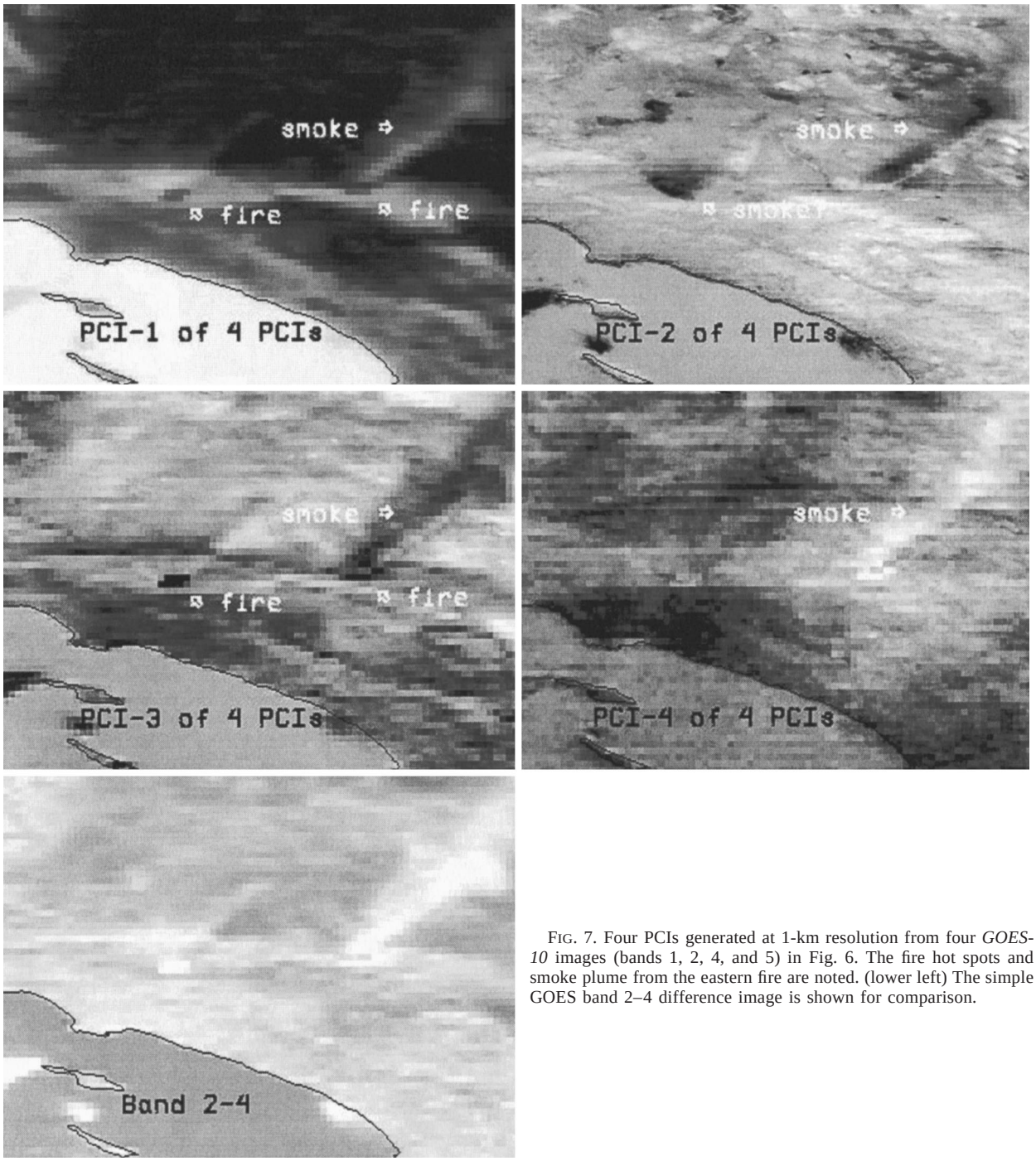

FIG. 7. Four PCIs generated at 1-km resolution from four *GOES-10* images (bands 1, 2, 4, and 5) in Fig. 6. The fire hot spots and smoke plume from the eastern fire are noted. (lower left) The simple GOES band 2–4 difference image is shown for comparison.

differences in the PCIs. The last two columns of Table 5 indicate that the PCIs, while contributing only a small part of the total explained variance, have sufficiently high SNRs to be useful.

2) SECOND CASE OF SMOKE AND FIRES

In this case, a large and destructive forest fire in the Los Alamos area of New Mexico is examined. Figure 8 contains four of the five *GOES-8* images (bands 1, 2, 4, and 5) for 2101 UTC 10 May 2000 at 2-km resolution, an intermediate resolution between the 1-km visible and 4-km infrared imagery. As in the previous case, the water vapor image (band 3) is not used or shown in this analysis, and all images are enhanced by contrast stretching. The dense smoke plume from the fire is better seen in the visible image (band 1, upper left-hand panel) than in any of the infrared images. (The assumed greater

TABLE 5. Explained variances and signal-to-noise ratios of PCIs generated from GOES bands 1, 2, 4, and 5 only at 2046 UTC 31 August 1999 for two fires in the mountains north of the Los Angeles basin in southern California.

PCI No.	Explained variance (%) and sign (negatives in parentheses) of GOEs band contributions				PCI explained variance (%)	PCI signal-to-noise ratio
	1	2	4	5		
1	7.1	45.3	24.4	23.2	96.5	195.8
2	87.4	(~0)	(8.2)	(4.4)	2.0	10.3
3	(5.2)	54.5	(16.9)	(23.4)	1.4	29.7
4	0.4	(0.2)	50.4	(49.0)	0.1	12.4

density of the smoke in the plume makes it more detectable in the visible portion of the spectrum than the smoke in the case just examined.) In the infrared images there are slight indications of the smoke as cooler (whiter) pixels. The fire hot spot covers several (dark) pixels in the shortwave image (band 2, upper right-hand panel).

Figure 9 contains the corresponding PCIs at 2-km resolution for this case. PCI-1 looks similar to all three infrared images (band 2, 4, and 5) in Fig. 8, with indications of the fire hot spot but a low signal from the smoke plume. PCI-2 (upper right-hand panel) and PCI-3 (middle left-hand panel) have better indications of the fire hot spot and smoke plume than the original bands. Table 6 indicates that both of these PCIs have large (positive) contributions from the visible image. (Note that the contributions from the visible band are positive, while in these PCIs the smoke is dark, as opposed to white smoke in the visible band. This is due to the inverse correlation between the visible and infrared bands. Because the infrared bands show the smoke and clouds as white, to reflect this inverse relationship and agree with the sense illustrated in Table 6, the visible imagery should be displayed with clouds and smoke appearing dark.) Last, the lower left-hand panel contains a GOES band 2 − 4 shortwave–longwave difference image for comparison to the PCIs. This image product shows both the fire hot spot and the smoke plume as white, but without the details already shown in the various PCIs.

In PCI-3 the smoke appears much darker than the

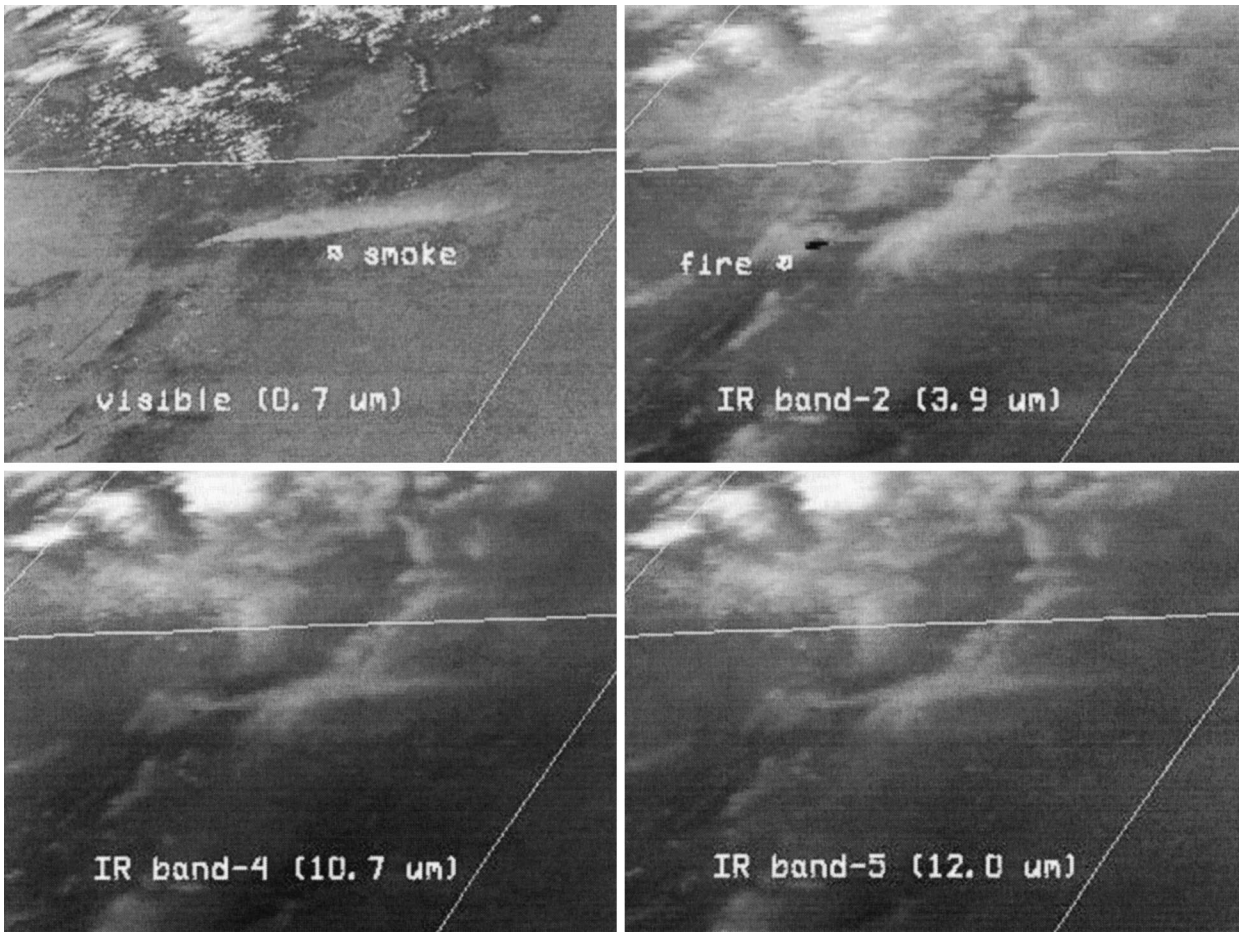

FIG. 8. *GOES-8* images for bands 1, 2, 4, and 5 at 2-km resolution showing smoke from the large Los Alamos, NM, forest fire at 2201 UTC 10 May 2000. The smoke plume and fire hot spot are noted on the band-1 and band-2 images, respectively. All images are contrast stretched to enhance features otherwise hard to discern.

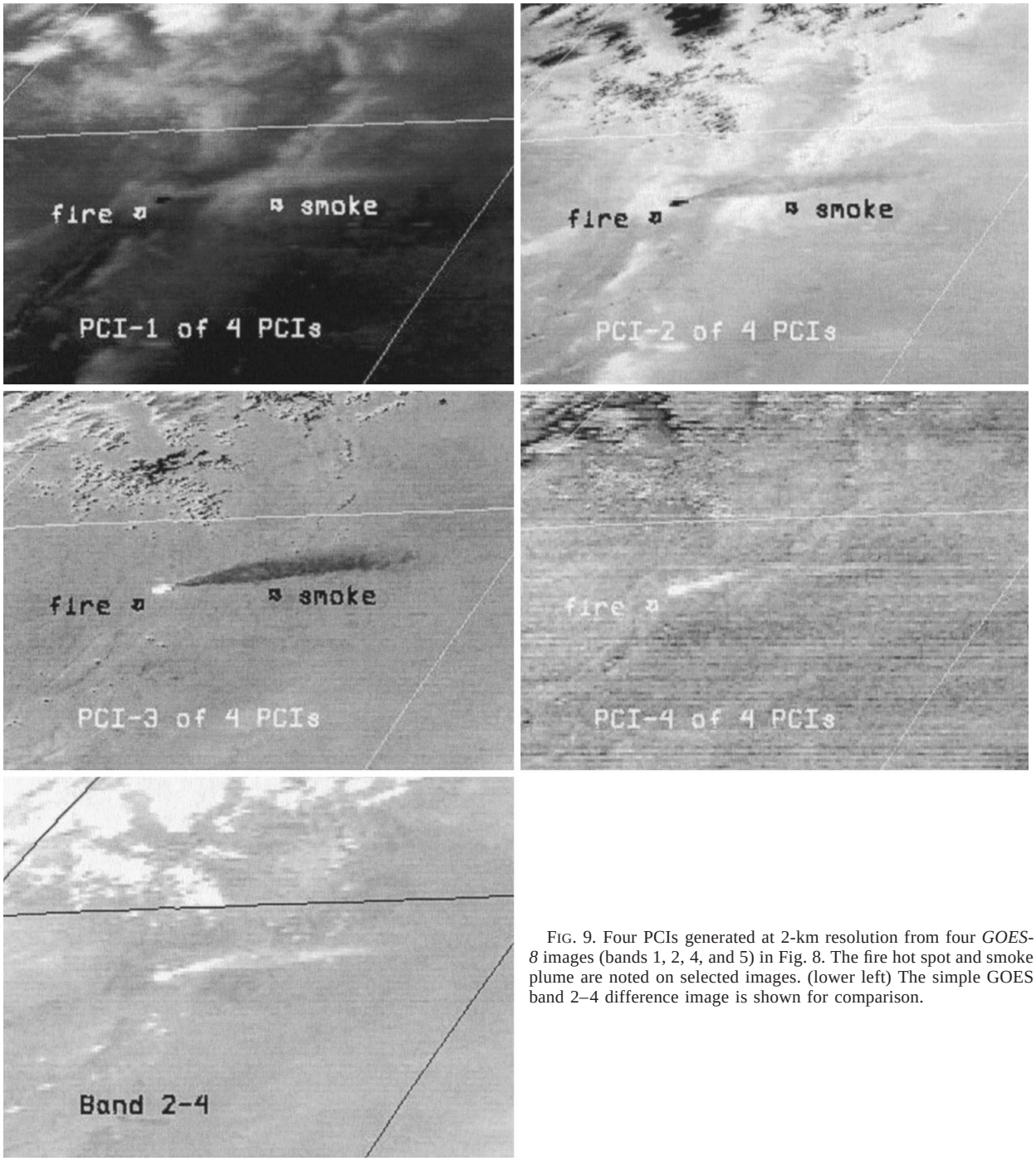

FIG. 9. Four PCIs generated at 2-km resolution from four *GOES-8* images (bands 1, 2, 4, and 5) in Fig. 8. The fire hot spot and smoke plume are noted on selected images. (lower left) The simple GOES band 2–4 difference image is shown for comparison.

surrounding background, which contrasts with the weaker indications of smoke in the original band images. PCI-4 (middle right-hand panel) shows the burning area and only the part of the smoke plume closer to the fire source. The remainder of the smoke plume is much harder to discern. This is an indication of the relative density of the smoke. The details of the smoke plume are not known, but the density can be assumed to decrease with distance downstream from the source due to mixing and settling of larger ash particles. [PCI-4 also shows detector-to-detector striping in GOES imagery (Hillger and Celone 1997), an undesirable feature that is a result of highly enhancing small differences between images.]

Although the PCIs for this case are somewhat similar to the ones for the first fire case, the main differences are the much larger contribution of the visible band to PCI-3 and the significant contribution of band 2 to PCI-

TABLE 6. Explained variances and signal-to-noise ratios of PCIs generated from GOES bands 1, 2, 4, and 5 only at 2201 UTC 10 May 2000 for the large Los Alamos, NM, forest fire.

PCI No.	Explained variance (%) and sign (negatives in parentheses) of GOES band contributions				PCI explained variance (%)	PCI signal-to-noise ratio
	1	2	4	5		
1	(1.2)	25.0	37.3	36.5	93.5	55.9
2	50.6	41.2	(2.7)	(5.5)	5.4	13.3
3	47.9	(32.7)	4.5	14.9	1.0	6.5
4	0.3	(1.1)	55.5	(43.0)	0.1	4.0

2. The increased contribution of the visible band supports the need for images from all of the bands (bands 1, 2, 4, and 5) for detecting fires and smoke. The PCIs, by highly enhancing multiband differences, show fire and smoke details more clearly. The last two columns of Table 6 reinforce the deduction that the PCIs, while contributing only a small part of the total explained variance, have sufficiently high SNRs to render them very useful.

3) THIRD CASE OF SMOKE AND FIRES

A final case is examined, not so much for the fire detection as for the large amount and wide extent of the smoke from those fires. In this case, numerous fires in Central America in the spring of 1998 caused widespread smoke coverage across much of the Gulf of Mexico that extended into the southeastern United States. Figure 10 contains images for 1531 UTC 9 May 1998 GOES bands 1, 2, 4, and 5 at 4-km resolution. The band-3 (water vapor) image is not used in the analysis for reasons discussed previously, and all images are enhanced by contrast stretching. The smoke is apparent in the visible image (band 1, upper left-hand panel), both where the smoke is dense closer to the source regions, as well as where it is less dense but in greater contrast with the low reflectance of the water background. The smoke is not as obvious in any of the infrared bands.

Figure 11 contains the corresponding PCIs at 4-km resolution for this case. PCI-2 (upper right-hand panel) and PCI-3 (lower left-hand panel) portray the strongest indications of the smoke. The lower spatial resolution (4 vs 1 km) of this case may degrade the ability to detect

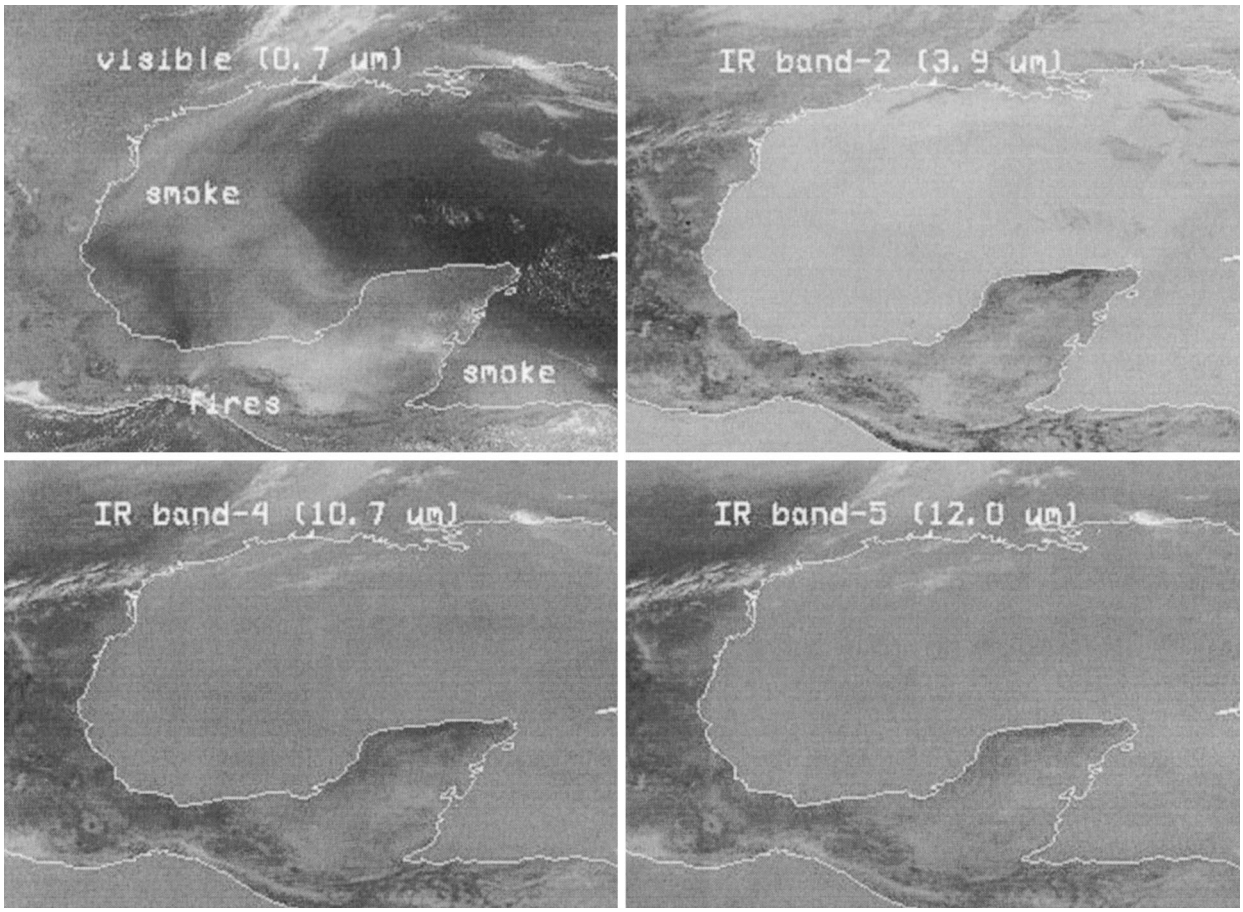

FIG. 10. *GOES-8* images for bands 1, 2, 4, and 5 at 4-km resolution showing the smoke over the Gulf of Mexico from numerous fires in Central America at 1531 UTC 9 May 1998. All images are contrast stretched to enhance features otherwise hard to discern.

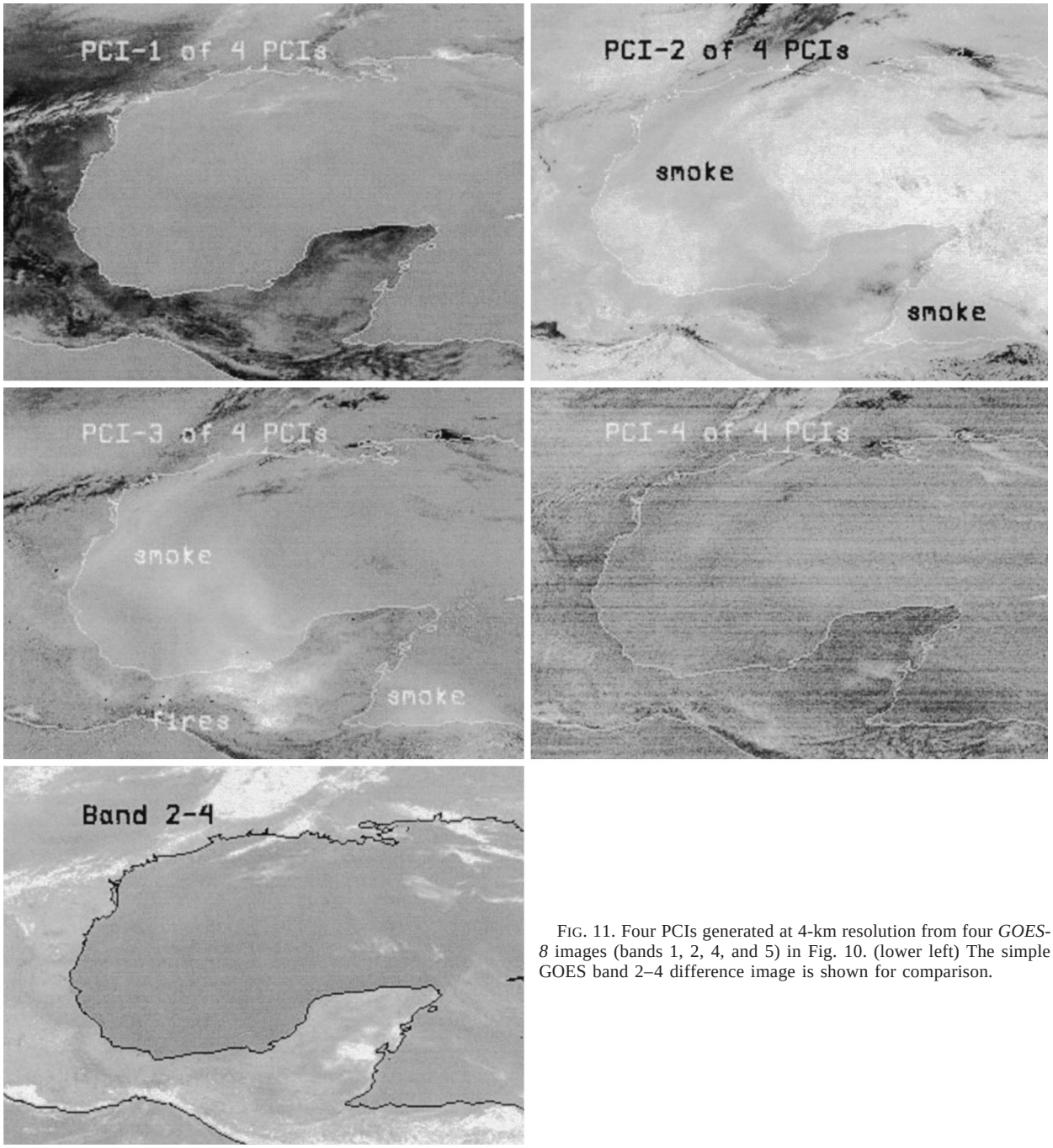

FIG. 11. Four PCIs generated at 4-km resolution from four *GOES-8* images (bands 1, 2, 4, and 5) in Fig. 10. (lower left) The simple GOES band 2–4 difference image is shown for comparison.

hot spots, but with a more homogeneous and cloud-free background, the smoke is more apparent than in the other fire and smoke cases where the terrain features varied widely. The fire locations are most apparent in PCI-3 as small black spots along the Gulf Coast of Mexico and into Central America. Table 7 indicates that PCI-3 depends strongly on the shortwave infrared image (band 2). The smoke that is apparent in PCI-2 and PCI-3 relies on the visible image in combination with other bands. (Note that the smoke is displayed as dark in PCI-3 for this case, as opposed to white in PCI-3 for the previous case. This is reflected in the opposite signs of the contributions of the bands in Tables 6 and 7. This can be remedied by inverting black to white in the display of PCI-3, which is equivalent to changing the signs of all the band contributions to that PCI.)

Also shown in the lower left-hand panel of Fig. 11 is a simple GOES band 2–4 difference image for comparison to the PCIs. This shortwave–longwave difference image shows some of the fire hot spots, but as with

TABLE 7. Explained variances and signal-to-noise ratios of PCIs generated from GOES bands 1, 2, 4, and 5 only at 1531 UTC 9 May 1998 for smoke over the Gulf of Mexico from numerous fires in Central America.

PCI No.	Explained variance (%) and sign (negatives in parentheses) of GOES band contributions				PCI explained variance (%)	PCI signal-to-noise ratio
	1	2	4	5		
1	~0	46.9	27.8	25.2	65.4	13.5
2	74.8	12.6	(5.4)	(7.2)	29.1	6.4
3	(24.9)	39.3	(10.4)	(25.4)	5.3	3.4
4	(0.2)	(1.1)	56.6	(42.2)	0.2	1.02

the PCIs they are hard to see at 4-km resolution. Smoke is not readily seen in this image difference product, nor is it detected by a band 5 − 4 difference (not shown). Small-sized smoke particles are best viewed in the visible band (band 1) in Fig. 10, or in PCIs 2 and 3, which utilize band 1.

The explained variances in the second to last column of Table 7 are much less biased toward PCI-1, with a much smaller variance (65.4%) than for all of the previous cases (all well over 90%). That smaller common variance is probably due to a basically cloud-free situation with smoke covering a larger fraction of the scene, putting more weight into the band differences in the higher-numbered PCIs. The SNRs in the last column are also generally smaller than in the previous cases, especially for PCI-4. The value of 1.02 (2% more signal than noise) indicates that there is little usable signal in this image above the significant image striping, a disadvantage in highly enhanced multiband images caused by unwanted instrument characteristics.

The three smoke and fire cases show the ability of PCIs to work on a wide range of spatial scales and different smoke situations. The PCIs for the three cases examined behaved similarly, but the combinations of bands utilized for the PCIs differed somewhat. In general it is better to have a visible band in combination with the infrared window bands to identify smoke, as indicated by the PCIs that showed smoke the best. This means that detection of smoke may be seriously hindered at night. Although not tested here on nighttime data, the PCI technique should indicate the bands that are best for smoke detection at night. Fire hot spots are also detected best by utilizing the shortwave band 2 in combination with infrared window bands. Differences in results between the cases are due to the different characteristics of the fire and smoke in each case, and the contrast of the fires and smoke to the image background and other image features.

4. Summary and conclusions

Principal component images (PCIs) are created by an eigenvector transformation of spectral band images from the five-band GOES imager. While this multispectral technique is normally applied to high-spatial resolution land remote sensing imagery, the application is herein made to lower-spatial resolution weather satellite imagery. The PCI transformation is a powerful tool that provides a new set of images that are linear combinations of the original spectral band images. This facilitates viewing the explained variance or signal in the available imagery. The band information is sorted into the PCIs, with higher-numbered PCIs containing much less of the explained variance, but information that is significant and above the noise level of the data. This allows both gross and more subtle features in the imagery to be seen. Some of the details in the PCIs are significant features in the earth's atmosphere and on the earth's surface that are not seen nearly as easily in the individual spectral band images.

In the cases examined, the PCIs were found to be very useful in detecting the extent and relative density of atmospheric dust, as well as forest and range fires and associated smoke plumes, by increasing the contrast of those features to the image background. Though not demonstrated here, the technique can similarly be used to detect or discriminate many other types of image features in multiband imagery: snow/cloud, volcanic ash (Hillger and Clark 2002a,b), cloud layers, land/water boundaries, cloud phase, and water vapor features in the atmosphere. The applications utilized the three GOES infrared window images (bands 2, 4, and 5) in dust situations, and included the visible image (band 1) in smoke situations. Typically, the GOES water vapor image is too opaque for detection of most low-level atmospheric phenomena and is of negligible utility for discrimination of features at the earth's surface.

From the cases used in this study, it is clear that PCIs have the ability to detect features in different situations and on different spatial scales. As shown elsewhere (Hillger and Clark 2002a,b), significant differences can occur between day and night with the change in the reflected component of solar radiation, an important factor in GOES bands 1 and 2. Clouds also complicate and limit the ability to detect desired features, just as they do for visible and infrared imagery. The interpretation of the PCIs is case dependent. Different features or different situations result in PCIs that are not identical combinations of the available bands. Because of these limitations, PCIs are not necessarily the best technique for direct operational applications, but can prove useful for determining combinations of the available band images for the detection of various atmospheric and surface features. The way to combine the bands may change, but there is benefit to be gained in knowing the bands that are of more value and those that are not of value. If the PCI technique shows that certain band combinations are preferable, those bands can be combined as specified by the PCIs to generate an operational product based on that training.

There are two conclusions from this study: 1) Atmospheric and surface features are more easily identi-

fied in PCIs than in the original spectral band images, even when enhanced by contrast stretching. The technique automatically combines redundant information based on the correlations between the bands, exposing band-difference information that is typically useful for analysis of dust and smoke. This technique proves to be especially important for detecting features that are best seen in multiband differences, as opposed to features easily seen in enhanced single-band images or simple two-band difference images. 2) The elimination of certain bands can be made either directly by inspection of the PCIs, discarding bands that do not contribute to the PCIs showing the desired features, or by including all available bands and letting the transformation process indicate the bands that are useful for detecting the desired features. This point was demonstrated by the two sets of PCIs generated for the first dust case, for which certain images were excluded from the analysis and the PCIs of significance were basically unchanged by excluding the unimportant bands.

The cases examined contained images from only one time period each, whereas the GOES imager normally collects imagery every 15 min. An image loop can add an extra dimension to the PCIs, allowing for the distinction of stationary versus moving features in satellite imagery. This would help distinguish between earth-fixed and dynamic atmospheric phenomena.

The PCI examples in this paper focused on applications to the five-band GOES imager, but have implications for other multispectral weather satellite imagery. The PCI technique is especially useful with the introduction to the satellite platform of new sensors with increased numbers of spectral bands. For example, 36 spectral bands are available from the Moderate Resolution Imaging Spectroradiometer (MODIS), flying aboard the polar-orbiting Earth Observation Satellites (EOS), one of which is already in orbit (Hillger and Clark 2002a). The new imager instrument on the first Meteosat Second Generation (MSG) satellite, to be launched in mid 2002, will provide 12 spectral bands from geostationary orbit. Images from these and other new instruments can be explored using PCIs to determine what atmospheric and surface features can be detected, and what bands are suitable for detection of those features.

Acknowledgments. This research was sponsored by NOAA Grant NA17RJ1228. Software for principal component image (PCI) analysis was developed for Regional and Mesoscale Meteorology Team (RAMMT) Advanced Meteorological Satellite Demonstration and Interpretation System (RAMSDIS; Molenar et al. 2000) satellite image analysis systems at the Cooperative Institute for Research in the Atmosphere (CIRA). Satellite image products resulting from PCI analysis are routinely generated on several in-house systems and at other selected sites where RAMSDIS is available. Doctor Mark DeMaria and Dr. Bernie Connell provided helpful reviews of the manuscript.

REFERENCES

Arking, A., and J. D. Childs, 1985: Retrieval of cloud cover parameters from multispectral satellite images. *J. Climate Appl. Meteor.,* **24,** 322–333.

Dills, P. A., D. W. Hillger, and J. F. W. Purdom, 1996: Distinguishing between different meteorological phenomena and land surface properties using the multispectral imaging capabilities of *GOES-8*. Preprints, *Eighth Conf. on Satellite Meteorology and Oceanography,* Atlanta, GA, Amer. Meteor. Soc., 339–342.

Ellrod, G. P., 1994: Detection and analysis of fog at night using GOES multispectral infrared imagery. NOAA Tech. Rep. NESDIS 75, 22 pp.

——, 1995: Use of the *GOES-8* ''split window'' infrared channels in the monitoring of low level moisture and African dust. Preprints, *21st Conf. on Hurricanes and Tropical Meteorology,* Miami, FL, Amer. Meteor. Soc., 634–636.

Fraser, R. S., 1976: Satellite measurement of mass of Sahara dust in the atmosphere. *Appl. Opt.,* **15,** 2471–2479.

Gauch, H. G., Jr., 1993: Prediction, parsimony, and noise. *Amer. Sci.,* **81,** 468–478.

Hillger, D. W., 1996a: Meteorological features from principal component image transformation of GOES imagery. *Proc. Int. Symp. on Optical Science, Engineering, and Instrumentation (GOES-8 and Beyond Conf.),* Denver, CO, SPIE, 111–121.

——, 1996b: Meteorological analysis using principal component image transformation of GOES imagery. *International Radiation Symposium—IRS '96: Current Problems in Atmospheric Radiation,* W. L. Smith and K. Stamnes, Eds., A. Deepak, 480–483.

——, 1999: GOES imager and sounder calibration, scaling, and image quality. NOAA Tech. Rep. NESDIS 93, 34 pp.

——, and T. H. Vonder Haar, 1988: Estimating noise levels of remotely sensed measurements from satellites using spatial structure analysis. *J. Atmos. Oceanic Technol.,* **5,** 206–214.

——, and P. J. Celone, 1997: A GOES image quality analysis system for the NOAA/NESDIS Satellite Operations Control Center. NOAA Tech. Rep. NESDIS 89, 32 pp.

——, and G. P. Ellrod, 2000: Detection of unusual atmospheric and surface features by employing principal component image transformation of GOES imagery. Preprints, *10th Conf. on Satellite Meteorology and Oceanography,* Long Beach, CA, Amer. Meteor. Soc., 461–464.

——, and J. Clark, 2002a: Principal component image analysis of MODIS for volcanic ash. Part 1: Most important bands and implications for future GOES imagers. *J. Appl. Meteor.,* **41,** 985–1001.

——, and ——, 2002b: Principal component image analysis of MODIS for volcanic ash. Part 2: Simulations of current GOES and GOES-M imagers. *J. Appl. Meteor.,* **41,** 1003–1010.

Holt, F. C., and S. R. Olson, 1999: *GOES Products and Services Catalog.* 2d ed. U.S. Department of Commerce, NOAA/NESDIS, 152 pp.

Lee, J. A., and V. P. Tchakerian, 1995: Magnitude and frequency of blowing dust on the southern High Plains of the United States. *Ann. Assoc. Amer. Geogr.,* **85,** 684–693.

Loughlin, W. P., 1991: Principal component analysis for alteration mapping. *Photogr. Eng. Remote Sens.,* **57,** 1163–1169.

Madura, D. P., J. M. Soha, W. B. Green, D. B. Wherry, and S. D. Lewis, 1978: Color enhancement of Landsat agricultural imagery. Jet Propulsion Laboratory Publ. 78-102, 68 pp.

Matson, M., and J. Dozier, 1981: Identification of subresolution high temperature sources using a thermal IR sensor. *Photogr. Eng. Remote Sens.,* **47,** 1311–1318.

Menzel, W. P., and J. F. W. Purdom, 1994: Introducing GOES-I: The

first of a new generation of geostationary operational environmental satellites. *Bull. Amer. Meteor. Soc.,* **75,** 757–781.
Molenar, D. A., K. J. Schrab, and J. F. W. Purdom, 2000: RAMSDIS contributions to NOAA satellite data utilization. *Bull. Amer. Meteor. Soc.,* **81,** 1019–1030.
Morrison, D. F., 1976: *Multivariate Statistical Methods.* McGraw-Hill, 415 pp.
Pollard, M. C., 1978: Guidelines for forecasting dust storms in the southern Great Plains. *Natl. Wea. Dig.,* **3,** 40–44.
Preisendorfer, R. W., 1988: *Principal Component Analysis in Meteorology and Oceanography*. Elsevier, 425 pp.
Takashima, T., and K. Masuda, 1987: Emissivities of quartz and Sahara dust powders in the infrared region (7–17 μm). *Remote Sens. Environ.,* **23,** 51–63.
Taylor, M. M., 1973: Principal components colour display of ERTS imagery. *Proc. Third Earth Resources Technology Satellite Symp.,* 1877–1897.
Weinreb, M. P., M. Jamison, N. Fulton, Y. Chen, J. X. Johnson, J. Bremer, C. Smith, and J. Baucom, 1997: Operational calibration of *Geostationary Operational Environmental Satellite-8* and *-9* imagers and sounders. *Appl. Opt.,* **36,** 6895–6904.